Optics Letters

Ultra-phase-stable infrared light source at the watt level

Simon Reiger,[1,2,3] Mikhail Mamaikin,[1] Dmitrii Kormin,[1] Keyhan Golyari,[1] Hadil Kassab,[1] Maximilian Seeger,[1,2] Volodymyr Pervak,[2] Nicholas Karpowicz,[1,2] and Thomas Nubbemeyer[1,2,*]

[1]Max Planck Institute of Quantum Optics, Hans-Kopfermann-Str. 1, 85748 Garching, Germany
[2]Ludwig Maximillian University Munich, Am Coulombwall 1, 85748 Garching, Germany
[3]simon.reiger@mpq.mpg.de
*thomas.nubbemeyer@physik.uni-muenchen.de

Received 20 October 2023; revised 19 January 2024; accepted 21 January 2024; posted 23 January 2024; published 14 February 2024

Ultrashort pulses at infrared wavelengths are advantageous when studying light–matter interaction. For the spectral region around 2 µm, multi-stage parametric amplification is the most common method to reach higher pulse energies. Yet it has been a key challenge for such systems to deliver waveform-stable pulses without active stabilization and synchronization systems. Here, we present a different approach for the generation of infrared pulses centered at 1.8 µm with watt-level average power utilizing only a single nonlinear crystal. Our laser system relies on a well-established Yb:YAG thin-disk technology at 1.03 µm wavelength combined with a hybrid two-stage broadening scheme. We show the high-power downconversion process via intra-pulse difference frequency generation, which leads to excellent passive stability of the carrier envelope phase below 20 mrad—comparable to modern oscillators. It also provides simple control over the central wavelength within a broad spectral range. The developed infrared source is employed to generate a multi-octave continuum from 500 nm to 2.5 µm opening the path toward sub-cycle pulse synthesis with extreme waveform stability.

https://doi.org/10.1364/OL.509905

Introduction. Few-cycle laser pulses are of high importance for observations of ultrafast light–matter interaction phenomena [1–5]. Coherent light sources capable of producing phase-stable radiation in the 2 m range, so called short wavelength infrared (SWIR), nowadays become popular for many reasons including strong-field ionization dynamics in gases [6] and nanostructures [7] and direct frequency-comb spectroscopy [8]. Furthermore, SWIR radiation facilitates the extension of the cutoff frequency in high harmonic generation [9–11] and enables efficient downconversion into the long-wave infrared range [12] for studying low-bandgap materials [13]. Ultimately, it has emerged as a powerful tool for the generation of super-octave-spanning continuum providing the synthesis of sub-cycle pulses at longer central wavelengths [14,15].

Few-cycle SWIR radiation has conventionally been derived through nonlinear downconversion of the pulses from titanium–sapphire lasers using intra-pulse difference frequency generation (IDFG), which inherently provides carrier envelope phase (CEP) stability [16]. Given the initially low average power of the resulting SWIR, post-amplification is usually performed. This is normally achieved by multi-stage optical parametric amplification (OPA) pumped by Yb- and Nd-based laser sources at millijoule pulse energies on the time scale of several to hundreds of picoseconds [17,18]. Current research demonstrates the generation of high-power SWIR radiation employing two-arm DFG to create a seed for OPA [19–21]. However, due to the interferometric nature of OPA schemes, the CEP fluctuations appear to be on the order of hundred milliradians despite active temporal and spatial synchronization.

Alternatively, Cr3+-doped II–VI materials, such as ZnS and ZnSe, can be used for obtaining highly CEP-stable few-cycle SWIR pulses directly from oscillators [22]. Boosting the pulse energy multi-pass amplification can be employed [9]; however, CEP stability of such laser systems was not yet shown.

Therefore, it is not trivial to combine high pulse energy, repetition rate, and CEP stability of SWIR pulses. In this Letter, we demonstrate an alternative concept for generating phase-stable radiation at 1.8 µm with above 1 W of power. We temporally compress the 1030 nm output of a thin-disk Yb:YAG amplifier down to nearly two cycles at the energy of 1 mJ utilizing a hybrid broadening scheme. These few-cycle pulses are directly used to generate CEP-stable SWIR radiation in a single beta barium borate (BBO) crystal via the IDFG process without any active stabilization. Such simple geometry also provides real-time tunability of the central wavelength from 1.6 to 2.2 µm. The CEP fluctuations of the generated SWIR radiation are measured via nonlinear upconversion, without the need for an octave-spanning spectrum like in standard self-referencing methods. Phase stability of less than 20 mrad highlights the advantage of our approach over conventional interferometric OPA schemes. Finally, we use the developed light source to produce a multi-octave continuum through the broadening in bulk and subsequent emission of a dispersive wave in a hollow-core capillary.

NIR laser system. The front-end of the laser system (Fig. 1) includes a home-built Yb:YAG regenerative amplifier seeded by a commercial fiber oscillator with pulses centered at 1030 nm

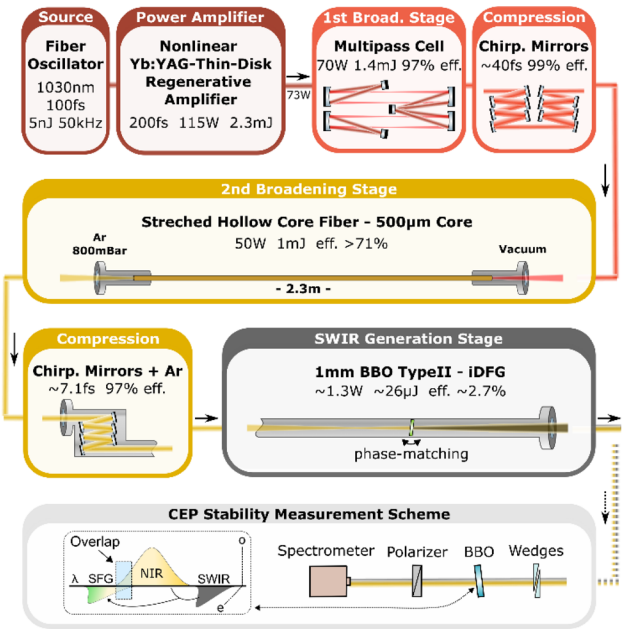

Fig. 1. Laser setup. Laser pulses at 1030 nm after two stages of nonlinear broadening and compression have 1 mJ pulse energy and 7.15 fs time duration. These pulses are focused into a 1 mm Type-II BBO generating SWIR output (~1.3 W at 1.8 µm). CEP stability of the emitted SWIR is analyzed through nonlinear upconversion with the residual NIR in BBO and interference in the spectral overlap region (see Supplement 1).

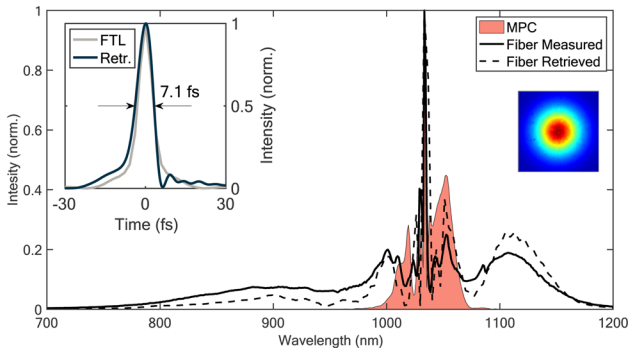

Fig. 2. Characterization of NIR pulses using a second-harmonic frequency-resolved optical gating (SHG-FROG) and a spectrometer. The shaded area represents the spectrum of the multipass-cell output, and the solid line is the spectrum after the hollow-core fiber. The dashed line corresponds to the reconstructed spectrum. The left inset displays the temporal profile and its Fourier limit. The right inset depicts the beam profile.

(MENLO FC1500-100-WG) [23]. The amplifier emits laser pulses with the energy of 2.3 mJ at 50 kHz repetition rate. One notable feature of this amplifier is non-stretched seed pulses, allowing for self-phase modulation (SPM) within the amplifier's cavity. As the result, we mitigate gain-narrowing and obtain pulses that are further compressed down to 200 fs with a compact chirped mirror compressor (CMC).

After the amplification, the pulses are guided to a hybrid nonlinear broadening setup, which consists of two stages. In the first stage, the beam propagates through a 4 f imaging multipass cell (MPC) in a vacuum chamber filled with 200 mbar of Argon [24]. The output spectrum is depicted in Fig. 2. As a result, the MPC and CMC (13 chirped mirrors, −225 fs^2 of GDD per mirror) deliver nearly-transform-limited pulses of ~40 fs duration with the overall transmission efficiency of 96%. The second broadening stage consists of a stretched 2.3-m-long hollow-core fiber (HCF, Few Cycle Inc.) with 500 µm inner core diameter. The input beam pointing is actively stabilized; the HCF itself is differentially pumped with ~800 mbar of Argon at the end of the capillary and vacuum at the entrance. The beam after the HCF passes through a CMC (3 pairs, −50 fs^2 of GDD per pair) providing 7.1 fs output pulses (Fig. 2) retrieved by a second-harmonic-generation frequency-resolved optical gating (SHG-FROG). For the complete data of the FROG retrieval, see Supplement 1 (Supplement 1). Our hybrid nonlinear compression setup has the total transmission of ~68% and utilizes the highest pulse energy among similar hybrid schemes [25]. Furthermore, this broadening tandem provides nearly ideal beam quality due to the mode cleaning property of the HCF. It is worth noting that to maintain a safe operation of the whole system, only ~73 W of the total laser power is sent to the hybrid broadening setup. We expect that a HCF with active cooling of the fiber entrance could support even higher power.

Generation of CEP-stable SWIR pulses. The few-cycle pulses after the hybrid broadening setup with more than 1 mJ of pulse energy cover the spectral range from 700 to 1200 nm. They are used for the generation of SWIR radiation around 2 µm via the IDFG process. For this purpose, we employ a single 1-mm-thick BBO crystal in the type-II phase-matching ($e - e \Rightarrow o$) configuration at a ~30° angle. As shown in [26], this type of phase-matching provides a stable output in terms of spectrum and CEP avoiding back-conversion or parasitic second-harmonic generation. At the same time, BBO provides high nonlinearity while having extremely high damage threshold and transparency over a broad spectral range. The NIR beam is focused into the BBO by a spherical mirror ($f = 4$ m) in a vacuum enclosure filled with Argon for GDD fine tuning via pressure adjustment. Its pressure can be adjusted for optimal compression of the input NIR pulses. The crystal is placed slightly after the focal point ($w_0 \sim 300$ µm at $1/e^2$) to avoid damage and partially compensate for self-focusing effects occurring in its volume. As shown in Fig. 3(a), the highest conversion efficiency of 2.7% is reached when the SWIR generation process is phase-matched for the central wavelength at 1.8 µm. The output SWIR power in this case is ~1.3 W, which corresponds to 26 µJ of pulse energy. The power was measured for 2 h, showing the variation of <1% RMS (see Supplement 1). The SWIR beam is separated from the residual NIR radiation by a dichroic beam splitter produced in our in-house coating facility. A wire-grid polarizer isolates the SWIR generated on the ordinary axis of the BBO from unwanted components on the orthogonal axis. It is worth noting that this unwanted radiation is emitted in the same spectral region on the extraordinary axis indicating simultaneous cascaded nonlinear processes [27] (see Supplement 1). The SWIR pulses were characterized using a third-harmonic-generation frequency-resolved optical gating (THG-FROG) setup. Figure 3(b) depicts the reconstruction of the temporal profile, indicating nearly optimal compression down to 30.6 fs (Fourier limit of 29fs, see SI).

This approach of SWIR generation using a single crystal offers not only stable high-power output but also simple control over the central wavelength via a slight adjustment of the phase-matching angle while in operation. The tuning of the central

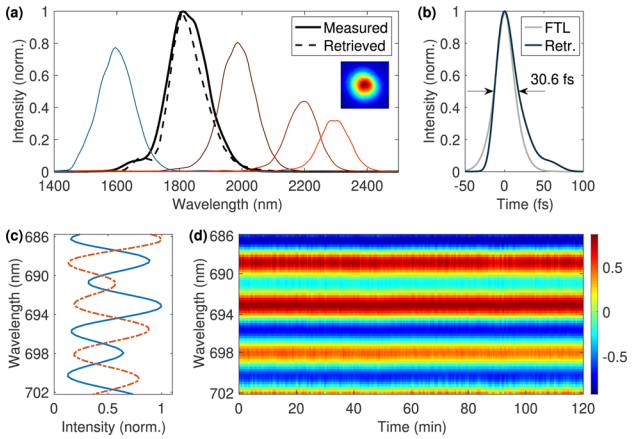

Fig. 3. (a) SWIR spectra generated using different phase-matching angles around 30°, with the solid lines representing measured spectra and the dashed line depicting the spectrum retrieved using THG-FROG. The inset displays the corresponding beam profile. (b) Retrieved temporal profile of the SWIR pulse at 1.8 µm and its Fourier limit. (c) Averaged interference fringes used for the CEP stability analysis; the dashed line shows a π-shift realized with a pair of wedges. (d) Interference fringes recorded continuously over 2 h. Additional subtraction of the π-shifted fringes was applied for improving the contrast. The overall CEP stability is equal to 19 mrad RMS.

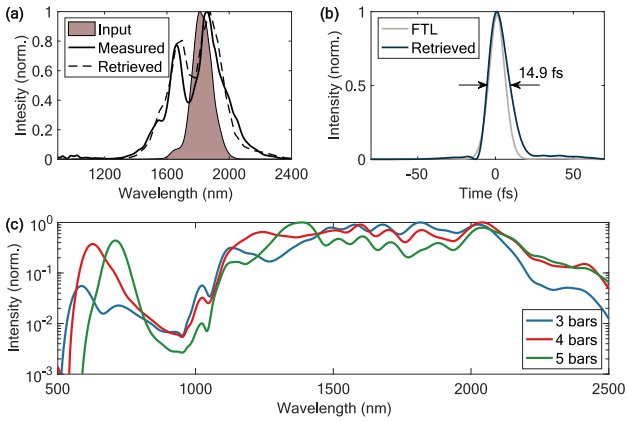

Fig. 4. (a) Input and output SWIR spectra after passing through the TiO_2 crystal. The solid line is the spectrum recorded by a spectrometer; the dashed line is the retrieved spectrum from the THG-FROG. (b) Temporal reconstruction of SWIR pulses with its Fourier limit. (c) Spectra measured after the broadening in a hollow-core fiber filled with 3–5 bars of krypton.

wavelength is depicted in Fig. 3(a), revealing just 20% reduction of the conversion efficiency within a range of ±200 nm from the maximum at 1.8 µm. Characterizing SWIR below 1.4 µm was not possible due to the limited transmission bandwidth of the dichroic beam splitter.

Due to the combination of simple geometry for the SWIR generation and its great power stability, high CEP stability is expected. To evaluate CEP fluctuations, we built a setup reminiscent of the electro-optic sampling method [28]. This way, the generated SWIR and co-propagating residual NIR beams are not separated by a beam splitter but are focused together onto a 100-µm-thick BBO crystal for sum-frequency generation (SFG). Phase-matching is adjusted for the SFG of the SWIR radiation and the long-wavelength part of the NIR emitting new spectral components around 700 nm (1800 nm [e] + 1145 nm [o] ⇒ 700 nm [e], see Fig. 1). This in turn interferes with the short wavelength part of the NIR radiation after adding a wire-grid polarizer for a projection to a common axis. Thus, the NIR phase cancels out in the interference signal, and the fringe pattern directly relates to the CEP variation of the SWIR radiation (See Supplement 1). Figure 3(c) demonstrates the control over the fringe position using a pair of wedges. The fringes were continuously recorded over 2 h by a spectrometer with the integration time of 6 ms, as depicted in Fig. 3(d). The analysis of the measured data yields the CEP noise of 19 mrad RMS. To our knowledge, these are the most phase-stable SWIR pulses with the average power exceeding 1 W. It is also important to note that inherent CEP stability of such a single-arm geometry IDFG process eliminates the issue of shot-to-shot phase variation coming from the time-jitter. Although the overall power conversion efficiency from the amplifier (73 W) to the SWIR pulses is only 1.8%, such CEP stability is not achievable in standard OPA schemes [19–21], where higher efficiency and average power can be reached.

Generation of multi-octave spectrum. High CEP stability is especially advantageous when aiming at the synthesis of single- and sub-cycle light pulses. The next step toward this direction is the generation of ultra-broad spectrum.

To demonstrate this capability, we present the spectral broadening of the generated SWIR pulses over 2.5 octaves. First, the full power of the 1.8 µm beam is focused onto a 500 µm titanium dioxide (TiO_2, Rutile) crystal by a silver off-axis parabolic mirror (for details, see Supplement 1). This material exhibits exceptional nonlinear characteristics within the SWIR range [22]. The SPM process in the crystal spectrally broadens the input beam covering the range from 1400 to 2300 nm while preserving 90% of the power (Fig. 4(a)). The pulses are characterized using a THG-FROG technique demonstrating the duration of 14.9 fs with the Fourier limit of 12 fs (Fig. 4(b), see Supplement 1 for the full retrieval). Therefore, the usage of a single TiO2 plate allows for direct temporal compression of the SWIR pulses down to nearly two cycles while exhibiting negligible power losses.

Afterwards, the broadening is performed in a 30-cm-long hollow-core capillary with 120 µm inner diameter filled with 3 to 5 bars of krypton. The resonant dispersive wave is emitted in the visible range indicating sufficient peak power of the input SWIR pulses for the soliton formation [29]. The bandwidth of the output supercontinuum covers 2.5 optical octaves, from 500 to 2500 nm (Fig. 4(c)). The dynamics of the dispersive wave can be controlled by varying the fiber pressure from 3 to 5 bars. Temporal shaping of such ultrabroadband spectra is typically performed using the pulse synthesis approach, where the full bandwidth is split into several channels for separate compression and following a coherent recombination [30,31].

Conclusions. In summary, we report a light source that relies on the advanced Yb:YAG thin-disk amplifier and provides 26 µJ of ultra-CEP-stable pulses at 1.8 µm with 50 kHz repetition rate. This was achieved by realization and thorough optimization of the two key concepts. The first is a hybrid two-stage broadening setup consisting of a multipass cell and a stretched hollow-core capillary. It provided 7.15 fs pulses with 1 mJ pulse energy centered around 1030 nm, which corresponds to the throughput of 68% and the temporal compression factor of 28. Another

important aspect of this work is the direct generation of the SWIR radiation in a single BBO crystal with watt-level output power. With the peak power over 800 MW, these pulses present an interesting tool for strong-field experiments that benefit from longer wavelengths such as high harmonic generation [21]. Our simple single-crystal geometry additionally provides the real-time tunability of the central wavelength of the generated pulses. This can be useful, for example, for studying molecular dynamics with laser-induced electron diffraction [32] or revealing additional information in extreme-ultraviolet spectroscopy [33].

The main feature of the generated SWIR pulses is their exceptional CEP stability with the fluctuations below 20 mrad RMS over 2 h. Such waveform stability is crucial when aiming at the synthesis of reproducible sub-cycle pulses for studying field-sensitive ultrafast phenomena. The extension toward the multi-octave spectrum needed for getting into the sub-cycle regime was realized through the highly efficient temporal compression in a TiO2 crystal and the subsequent spectral broadening in the hollow-core capillary.

We foresee that such light source can serve as a new platform for precise attosecond experiments [34] and the advancement of light-field-driven electronics [35].

Funding. Max-Planck-Gesellschaft; Munich-Centre for Advanced Photonics; Air Force Office of Scientific Research (FA9550-16-1-0073).

Acknowledgment. The authors thank Moritz Ueffing, Clemens Jakubeit, Matthew Weidman, Qingcao Liu, Najd Altwaijry, and Enrico Ridente for their assistance in the laboratory and Prof. Ferenc Krausz for supporting this research project.

Disclosures. The authors declare no conflicts of interest.

Data availability. Data underlying the results presented in this paper may be obtained from the authors upon reasonable request.

Supplemental document. See Supplement 1 for supporting content.

REFERENCES

1. T. Brabec and F. Krausz, Rev. Mod. Phys. **72**, 545 (2000).
2. R. Huber, F. Tauser, A. Brodschelm, *et al.*, Nature **414**, 286 (2001).
3. P. Gaal, W. Kuehn, K. Reimann, *et al.*, Nature **450**, 1210 (2007).
4. F. Schlaepfer, M. Lucchini, S. A. Sato, *et al.*, Nat. Phys. **14**, 560 (2018).
5. I. Pupeza, M. Huber, M. Trubetskov, *et al.*, Nature **577**, 52 (2020).
6. A. Chew, N. Douguet, C. Cariker, *et al.*, Phys. Rev. A **97**, 031407 (2018).
7. G. Herink, D. R. Solli, M. Gulde, *et al.*, Nature **483**, 190 (2012).
8. S. Vasilyev, V. Smolski, J. Peppers, *et al.*, Opt. Express **27**, 35079 (2019).
9. V. E. Leshchenko, B. K. Talbert, Y. H. Lai, *et al.*, Optica **7**, 981 (2020).
10. J. Pupeikis, P.-A. Chevreuil, N. Bigler, *et al.*, Optica **7**, 168 (2020).
11. T. Gaumnitz, A. Jain, Y. Pertot, *et al.*, Opt. Express **25**, 27506 (2017).
12. S. Vasilyev, I. S. Moskalev, V. O. Smolski, *et al.*, Optica **6**, 111 (2019).
13. M. Schlecht, M. Knorr, C. P. Schmid, *et al.*, Sci. Adv. **8**, eabj5014 (2022).
14. E. Ridente, M. Mamaikin, N. Altwaijry, *et al.*, Nat. Commun. **13**, 1111 (2022).
15. P. Steinleitner, N. Nagl, M. Kowalczyk, *et al.*, Nat. Photonics **16**, 512 (2022).
16. C. Manzoni, G. Cerullo, and S. De Silvestri, Opt. Lett. **29**, 2668 (2004).
17. E. Ridente, M. Weidman, M. Mamaikin, *et al.*, Optica **7**, 1093 (2020).
18. R. Budriūnas, T. Stanislauskas, and A. Varanavičius, J. Opt. **17**, 094008 (2015).
19. M. F. Seeger, D. Kammerer, J. Blöchl, *et al.*, Opt. Express **31**, 24821 (2023).
20. M. Neuhaus, H. Fuest, M. Seeger, *et al.*, Opt. Express **26**, 16074 (2018).
21. I. Sytcevich, A.-L. Viotti, C. Guo, *et al.*, Opt. Express **30**, 27858 (2022).
22. M. Kowalczyk, N. Nagl, P. Steinleitner, *et al.*, Optica **10**, 801 (2023).
23. M. Ueffing, R. Lange, T. Pleyer, *et al.*, Opt. Lett. **41**, 3840 (2016).
24. M. Ueffing, S. Reiger, M. Kaumanns, *et al.*, Opt. Lett. **43**, 2070 (2018).
25. L. Lavenu, M. Natile, F. Guichard, *et al.*, Opt. Express **27**, 1958 (2019).
26. H. Fattahi, A. Schwarz, S. Keiber, *et al.*, Opt. Lett. **38**, 4216 (2013).
27. Y. Yin, X. Ren, A. Chew, *et al.*, Sci. Rep. **7**, 11097 (2017).
28. S. Keiber, S. Sederberg, A. Schwarz, *et al.*, Nat. Photonics **10**, 159 (2016).
29. J. C. Travers, T. F. Grigorova, C. Brahms, *et al.*, Nat. Photonics **13**, 547 (2019).
30. A. Wirth, M. T. Hassan, I. Grguras, *et al.*, Science **334**, 195 (2011).
31. G. Cirmi, R. E. Mainz, M. A. Silva-Toledo, *et al.*, Laser Photonics Rev. **17**, 2200588 (2023).
32. C. I. Blaga, J. Xu, A. D. DiChiara, *et al.*, Nature **483**, 194 (2012).
33. C. Vozzi, M. Negro, F. Calegari, *et al.*, Nat. Phys. **7**, 822 (2011).
34. D. Zimin, N. Karpowicz, M. Qasim, *et al.*, Nature **618**, 276 (2023).
35. D. Hui, H. Alqattan, S. Zhang, *et al.*, Sci. Adv. **9**, eadf1015 (2023).